Journal of Pharmaceutical Analysis 14 (2024) 100950

Contents lists available at ScienceDirect

Journal of Pharmaceutical Analysis

journal homepage: www.elsevier.com/locate/jpa

Original article

MGMT activated by Wnt pathway promotes cisplatin tolerance through inducing slow-cycling cells and nonhomologous end joining in colorectal cancer

Haowei Zhang [a, b], Qixin Li [a, b], Xiaolong Guo [b], Hong Wu [a], Chenhao Hu [a, c], Gaixia Liu [a, b], Tianyu Yu [a, b], Xiake Hu [a, b], Quanpeng Qiu [a, b], Gang Guo [b, c], Junjun She [a, b, c, *], Yinnan Chen [b, c, **]

[a] Department of General Surgery, The First Affiliated Hospital of Xi'an Jiaotong University, Xi'an, 710061, China
[b] Center for Gut Microbiome Research, Med-X Institute, The First Affiliated Hospital of Xi'an Jiaotong University, Xi'an, 710061, China
[c] Department of High Talent, The First Affiliated Hospital of Xi'an Jiaotong University, Xi'an, 710061, China

ARTICLE INFO

Article history:
Received 13 September 2023
Received in revised form
31 January 2024
Accepted 7 February 2024
Available online 10 February 2024

Keywords:
Colorectal cancer
MGMT
Chemotherapy resistance
Slow-cycling cells
Nonhomologous end joining
Wnt pathway

ABSTRACT

Chemotherapy resistance plays a pivotal role in the prognosis and therapeutic failure of patients with colorectal cancer (CRC). Cisplatin (DDP)-resistant cells exhibit an inherent ability to evade the toxic chemotherapeutic drug effects which are characterized by the activation of slow-cycle programs and DNA repair. Among the elements that lead to DDP resistance, O^6-methylguanine (O^6-MG)-DNA-methyltransferase (MGMT), a DNA-repair enzyme, performs a quintessential role. In this study, we clarify the significant involvement of MGMT in conferring DDP resistance in CRC, elucidating the underlying mechanism of the regulatory actions of MGMT. A notable upregulation of MGMT in DDP-resistant cancer cells was found in our study, and MGMT repression amplifies the sensitivity of these cells to DDP treatment *in vitro* and *in vivo*. Conversely, in cancer cells, MGMT overexpression abolishes their sensitivity to DDP treatment. Mechanistically, the interaction between MGMT and cyclin dependent kinase 1 (CDK1) inducing slow-cycling cells is attainted via the promotion of ubiquitination degradation of CDK1. Meanwhile, to achieve nonhomologous end joining, MGMT interacts with XRCC6 to resist chemotherapy drugs. Our transcriptome data from samples of 88 patients with CRC suggest that MGMT expression is co-related with the Wnt signaling pathway activation, and several Wnt inhibitors can repress drug-resistant cells. In summary, our results point out that MGMT is a potential therapeutic target and predictive marker of chemoresistance in CRC.

1. Introduction

Platinum-based chemotherapy is employed for the therapy of numerous types of solid malignancies inclusive of colorectal cancer (CRC) [1]. Cisplatin (DDP) exerts anti-tumor effects through the interaction with DNA to mostly cause intra-strand crosslink adducts, which induce cell cycle arrest and pro-apoptotic signal transduction pathways [2]. Several patients are inherently or acquiredly resistant to DDP or other platinum-based drugs even with preliminary therapeutic success, which is a serious dilemma for clinical treatment [3] and a major cause of mortality among patients with CRC. DDP resistance take place due to complicated reasons, which include impaired drug uptake processes, expanded drug efflux, drug breakdown, activation of repair mechanisms, reduced inter- or intra-strand DNA cross-linking, and increased pro-survival pathway activation or inhibition of pathways that promote cell apoptosis [4]. Although a cluster of signaling effectors having been recognized as indicators of DDP resistance, most of the studies either lacked an evaluation of clinical relevance or did not elucidate how to reverse drug resistance in CRC therapy. Thus, the specified molecular mechanisms of platinum-based drug resistance remain elusive, and overcoming chemotherapy resistance in CRC is critical.

* Corresponding author. Department of General Surgery, The First Affiliated Hospital of Xi'an Jiaotong University, Xi'an, 710061, China.
** Corresponding author. Center for Gut Microbiome Research, Med-X Institute, The First Affiliated Hospital of Xi'an Jiaotong University, Xi'an, 710061, China.
E-mail addresses: sjuns@sina.com (J. She), superyaami@163.com (Y. Chen).

https://doi.org/10.1016/j.jpha.2024.02.004

Tumor cells that can break out the exceedingly selective stress of antiproliferative agents are characterized as drug-tolerant persistence (DTP) cells [5]. The characteristic of DTP cells is to activate slow-cycle programs [6,7]. Cancer cells that grow slowly or are arrested in the cell cycle are much less sensitive to chemotherapeutic agents compared to those presenting with rapid proliferation. A study on patients with CRC demonstrated that tumors enriched in slow-cycling cells exhibit stronger chemotherapy resistance [8]. In cell cycle regulation [9], checkpoint activation [10], and DNA damage repair [11], cyclin dependent kinase 1 (CDK1) plays a crucial role. During the transition from G1 to S phase, CDK1 expression is high in cycling cells and cells that are exiting quiescence [12]. The regulation of the expression or CDK1 activity is crucial for the development of slow-cycling cells. CDK1 protein is inherently unstable and is regulated via the ubiquitin-mediated degradation process [13]. To enhance the effectiveness of antiproliferative drugs [14], it has been proposed to drive slow cycling cancer cells to re-enter the cell cycle for proliferation, thus enhancing the response to chemotherapeutic agents.

DDP induces DNA double-strand breaks (DSBs) [15], the most severe type of DNA injury. Without repair, these breaks can lead to cell death [16]. DDP-resistant cells can repair DNA damage to withstand the effects of DDP. DSB repair primarily depends on two mechanisms: nonhomologous end joining (NHEJ) and homologous recombination (HR) [17]. In the cell cycle, NHEJ mainly occurs in the G0/G1 and G2 phases, whereas HR occurs in the S and G2 phases of the cell cycle [18]. NHEJ is a significant intracellular mechanism for repairing DSBs [19]. NHEJ generally occurs through binding of the Ku70-Ku80 complex to the DSB terminus, which subsequently recruits other interacting proteins and mediates the terminus attachment [20]. NHEJ is of great significance in the preservation of the stability of the DDP-resistant cell genome.

O^6-methylguanine (O^6-MG)-DNA-methyltransferase (MGMT) encodes the DNA-repair protein O^6-alkylguanine (O^6-AG) DNA alkyltransferase. In cancer research, MGMT is of unique interest due to the fact it performs a fundamental position in temozolomide treatment for glioma [21]. When treated with O^6-alkylating agents such as temozolomide, tumor cells with MGMT overexpression can remove alkylating lesions at position O^6 of guanine, rescuing tumor cells from apoptosis and eventually leading to drug resistance. In the first-line treatment of CRC, platinum-based chemotherapy is utilized as a DNA alkylating agent [22]; however, the role and the MGMT mechanism in DDP chemotherapy for colon cancer remains poorly elucidated.

The regulation of MGMT expression is primarily through epigenetic modifications [23]. The methylation of the MGMT promoter in tumors results in the silencing of MGMT expression and enhances the response to chemotherapy [24]. Conversely, promoter methylation removal can eventually lead to tumor cell resistance to alkylating agents. Furthermore, a negative modulation of the Wnt signal cascade activity represses MGMT expression and sensitizes tumor cells to chemotherapy with alkylating agents [25]. In intestinal crypt cell division, Wnt/β-catenin signaling performs a vital position. Thus, the mutations and mis-regulation of Wnt/β-catenin signaling are relevant to colorectal tumorigenesis. The Wnt ligand represses GSK3β activity via the interaction with coiled-coil receptors and LRP5/LRP6 co-receptor transduction, eventually leading to β-catenin protein accumulation in the nucleus [26]. The Wnt/β-catenin signaling cascade is activated abnormally in colorectal cancer, leading to both the development and progression of the disease, as well as resistance to cancer treatments [27]. Wnt signaling suppression enhances chemotherapeutic drug sensitivity to tumor cells [28,29]. However, to our knowledge, the regulatory relationship between the Wnt pathway and MGMT in CRC remains elusive.

Our results suggest that CRC cells with higher MGMT expression were resistant to DDP treatment. Inhibition or knockdown of MGMT increased the sensitivity of CRC cells to DDP treatment, whereas MGMT overexpression led to DDP resistance. Additionally, MGMT expression in CRC-resistant cells is positively correlated with key factors of the Wnt pathway, and MGMT-mediated DDP resistance is inextricably due to CDK1 and XRCC6 interaction.

2. Materials and methods

2.1. Clinical tissue samples

Tumor samples were collected from patients with CRC who underwent surgical resection at the First Affiliated Hospital of Xi 'an Jiaotong University, Xi'an, China. These CRC tissue samples were immediately frozen in liquid nitrogen and stored at −80 °C for subsequent experiments. The cases were collected according to a clear pathological diagnosis and patient consent. This study was approved by the Internal Review and Science Committee of the First Affiliated Hospital of Xi'an Jiaotong University (Approval No.: XJTU1AF2023LSK-2023-218).

2.2. Cell culture

All cells were identified using a short tandem repeat analysis before being used for experimental studies. HCT116, SW480, MC38, and HEK293T cells were cultured in Dulbecco's modified Eagle medium (DMEM) (Gibco; Thermo Fisher Scientific Inc., Waltham, MA, USA) supplemented with 10% fetal bovine serum (FBS) (Gibco; Thermo Fisher Scientific Inc.) without antibiotics. All these cell lines were maintained at 37 °C with 5% CO_2 in a humidified incubator.

2.3. DDP-resistant cells

HCT116 cells were exposed to an initial DDP concentration of 2 μg/mL in DMEM plus 10% FBS. The surviving cell population was grown to 80% confluence and passaged twice over nine days to ensure viability. The half maximal inhibitory concentration (IC_{50}) values for DDP were measured using the thiazolyl blue tetrazolium bromide (MTT) assay every month. Cells were exposed to half dose of the IC_{50}. Drug-resistant cell lines were obtained after a six-month stimulation. HCT116 cells were then continuously maintained with 5 μg/mL DDP for three months to stabilize it. The control parental cells were passaged in parallel.

2.4. IC_{50} assay

Cells were seeded into 96-well plates at a density of 5×10^3 cells/well. The drug was diluted in a gradient, and the diluted drug was added to the 96-well plate. Cells were incubated in a 5% CO_2 incubator at 37 °C for 48 h. Then, a 10 μL of MTT solution (5 mg/mL) was added to each well and cells were incubated for another 4 h. After discarding the incubation solution, 100 μL of dimethyl sulfoxide (DMSO) was added to each well to fully dissolve the precipitate, and the optical density (OD) value at 490 nm was detected using an automatic microplate reader (Tecan, Männedorf, Switzerland). The data were analyzed and the IC_{50} curve was plotted.

2.5. Cell proliferation assay

Cells were seeded into 96-well plates at a density of 2×10^3 cells/well, and 10 μL of MTT solution (5 mg/mL) was added after 24, 48, 72, 96, 120, or 148 h. After continuing incubation for 4 h, the medium in the wells was discarded, and 100 μL of DMSO was added to dissolve the precipitate. After the precipitate was dissolved, the absorbance of

the wells was measured at 490 nm. The growth curve was then plotted according to the measured absorbance.

2.6. SA-β-galactosidase (β-gal) staining

Cells were grown in 24-well plates, the cell culture medium was discarded, and cells were washed once with phosphate-buffered saline (PBS). The wells were added with 4% paraformaldehyde, and the cells were fixed at room temperature for 15 min. The staining working solution (Beyotime, Shanghai, China) was configured according to the manufacturer's instructions. Cells were incubated overnight at 37 °C after adding the staining working solution to each well. The stained cells were observed and photographed under ordinary light microscope (Leica, Wetzlar, Germany).

2.7. 5-Bromo-2′-deoxyuridine (BrdU) assay

Cells were seeded in 48-well plates and cultured for 2 h after adding BrdU (3 μg/mL) to the culture medium. The cells were completely submerged with cooled 4% paraformaldehyde and fixed for 30 min at room temperature after discarding the medium. The fixative was discarded, and the cells were washed three times with PBS. Then, 2 M hydrochloric acid was added to the wells, and the cells were incubated at 37 °C for 30 min. Hydrochloric acid was removed, and cells were washed with PBS three times. The cells were washed twice with 0.1 M $Na_2B_4O_7$ at room temperature. The treated cells were then incubated with an anti-BrdU antibody (1:300; Santa Cruz Biotechnology, Santa Cruz, CA, USA) overnight at 4 °C. Cells were incubated with Cy3-coupled secondary antibody (1:300; Proteintech, Wuhan, China) for 1 h at room temperature after washing three times. Cells were washed and stained with 4′,6-diamidino-2-phenylindole (DAPI), and the nuclei were visualized under a fluorescent microscope (Nikon, Tokyo, Japan).

2.8. Ki67 fluorescence intensity assay

Cells were washed once with PBS containing 1% FBS (FB). Cells were then resuspended using a fixation/permeabilization buffer (Invitrogen, Carlsbad, CA, USA) for 30–60 min at room temperature. Cells were subsequently washed with a permeabilization buffer (Invitrogen) and incubated with a Ki67 antibody (1:200; Proteintech) for 1 h at 4 °C. Thereafter, cells were incubated with CoraLite594-coupled fluorescent secondary antibody (1:250; Proteintech) for 30 min at 4 °C, after being washed twice with FB. Cells were resuspended with a permeabilization buffer, and fluorescence intensity was measured using flow cytometry (Agilent Technologies, Santa Clara, CA, USA).

2.9. Apoptosis assay

Using ethylenediamine tetraacetic acid (EDTA)-free trypsin, cells were collected. A negative control group, a positive control group, and an experimental group were set up for the assay. Cells were washed with PBS and counted, and 5×10^5 resuspended cells were stained using the FITC-Annexin V/PI Apoptosis Kit (UElandy, Suzhou, China). After incubation, cells were resuspended by directly adding 1× annexin V binding buffer and immediately detected via flow cytometry.

2.10. RNA extraction, quantitative real-time polymerase chain reaction (RT-qPCR), and RNA-sequencing (RNA-seq) analysis

Total RNA was extracted from the cell lines using TRIzol reagent (Solarbio, Beijing, China) according to standard protocols. RNA was converted to complementary DNA (cDNA) using the Evo M-MLV RT Mix Kit with gDNA Clean for qPCR (Accurate Biotechnology, Changsha, China). To perform RT-qPCR, Agilent Aria real-time system (Agilent Technologies) was used. Glyceraldehyde-3-phosphate dehydrogenase (GAPDH) was used as an internal reference for messenger RNA (mRNA) quantification. Primer sequences are demonstrated in Table 1. Each experiment was repeated three times.

The RNA-seq platform used in the cell lines is TruSeq mRNA-seq and the RNA-seq platform used in the patient tumor tissue is NovaSeq6000. RNA-seq data were filtered through rapid quality control (www.bioinformatics.babraham.ac.uk/projects/fastqc/, accessed March 28, 2022) using Cutadapt to remove adapters and low-quality bases. Gene-level quantification was then performed using Salmon, and the DESeq2 R package was used to detect differentially expressed genes with a log-transformed fold change > 2 and a Benjamini–Hochberg adjusted *P*-value < 0.1. Metascape was used for the enrichment analysis of pathways and biological processes with differentially expressed genes [30–32].

2.11. Western blot assay

Cells were lysed with radioimmunoprecipitation assay (RIPA) lysis buffer (Beyotime) containing protease and phosphatase inhibitors. By employing the Enhanced BCA Protein Assay Kit (Beyotime), protein concentration was detected. Cell lysates were denatured with 5× sodium dodecyl sulfate (SDS) loading buffer for 5 min at 95 °C. Equal amounts of proteins were added to the sodium dodecyl-sulfate polyacrylamide gel electrophoresis (SDS-PAGE) and then transferred to polyvinylidene fluoride (PVDF) blotting membranes (Millipore, Billerica, MA, USA). Next, PVDF blotting membranes were blocked with 5% nonfat milk for 2 h at room temperature and blocked with a mixture of proteins targeting MGMT (1:2000; Proteintech), poly (adenosine diphosphate (ADP)-ribose) polymerase 1 (PARP1) (1:2000; Proteintech), cleaved PARP1 (1:1000; Cell Signaling Technology, Inc., Danvers, MA, USA), caspase-3 (1:1000; Cell Signaling Technology, Inc.), cleaved caspase-3 (1:1000; Cell Signaling Technology, Inc.), caspase-7 (1:1000; Cell Signaling Technology, Inc.), cleaved caspase-7 (1:1000; Cell Signaling Technology, Inc.), cyclin D1 (1: 1000; Cell Signaling Technology, Inc.), beta catenin (1:10,000; Proteintech), cyclin dependent kinase inhibitor 1A (P21) (1:1000; Proteintech), cyclin dependent kinase inhibitor 2A (P16) (1:1000; Proteintech), CDK1 (1:1000; Proteintech), XRCC6 (1:10000; Proteintech), HA tag (1:5000; Proteintech), ubiquitin (1:2000; PTM Bio, Hangzhou, China), GAPDH (1:10000; Proteintech), and α-tubulin (1:10000; Proteintech) at 4 °C overnight. The membranes were then washed three times with Tris-buffered saline with Tween-20 (TBST) and incubated with the corresponding secondary goat-anti-rabbit IgG (1:10000; Proteintech) or goat-anti-mouse IgG antibody (1:10000; Proteintech) for 2 h at room temperature. After rewashing, protein bands were detected with a chemiluminescent horseradish peroxidase (HRP) substrate (Millipore) in the ChemiDoc™ MP system (Bio-Rad, Hercules, CA, USA).

Table 1
Primers used in quantitative real-time polymerase chain reaction (RT-qPCR).

Primer names	Sequences
MGMT+	5′-ACCGTTTGCGACTTGGTACTT-3′
MGMT−	5′-GGAGCTTTATTTCGTGCAGACC-3′
GAPDH+	5′-AAGGTCGGAGTCAACGGATTTGGT-3′
GAPDH−	5′-AAGCTTCCCGTTCTCAGCCTTGAC-3′
CDK1+	5′-CAGAGCTTTGGGCACTCCCAATAA-3′
CDK1−	5′-CCAGAAATTCGTTTGGCTGGATCA-3′

MGMT: O^6-methylguanine (O^6-MG)-DNA-methyltransferase; GAPDH: glyceraldehyde-3-phosphate dehydrogenase; CDK1: cyclin dependent kinase 1.

2.12. Stable short hairpin RNA (shRNA) transfection

To construct a recombinant plasmid, the shRNAs were inserted into the plasmid vector pLKO.1. The shRNA sequences are demonstrated in Table 2. The recombinant plasmid vector pLKO.1 and helper plasmid vectors pVSVG, pREV, and pGAG were conjugated with Lipofectamine 2000 (Invitrogen) and transfected into 293T cells. Supernatants from the 293T cells were collected after 48 and 72 h, and the virus was concentrated with PEG8000. The HCT116-DDP cells were infected with lentivirus, and polybrene (Solarbio) was added to improve infection efficiency. The cells were screened with puromycin (2 μg/mL) for 48 h after infection.

2.13. Stable transfection of overexpression plasmids

The coding DNA sequence region of the MGMT was amplified through high-fidelity PCR and inserted into the plasmid vector pLVX-HA-IRES-Neo. The primer sequences were as follows: MGMT-HA+, 5′-CGGAATTCaccgtttgcgacttggtact-3′, MGMT-HA−, and 5′-CCCTCGAGgtttcggccagcaggcgg-3'. The recombinant pLVX-HA-IRES-Neo vector plasmid, the helper vector psPAX2, and pMD2.G were mixed with Lipofectamine 2000 and transfected into 293T cells. Supernatants were collected at 48 and 72 h, and PEG8000 was added to concentrate the virus. HCT116, SW480, and MC38 cells were infected with lentivirus and cells were screened with G418 (Solarbio) for 48 h to obtain stable transfected cell lines.

2.14. Immunohistochemistry staining

C57BL/6J mice subcutaneous tumor tissue sections were dewaxed and hydrated. To inactivate the endogenous enzyme, an appropriate amount of endogenous peroxidase blocker was added to the tissue sections and incubated for 10 min at room temperature. The tissue sections were immersed in citrate buffer for antigenic epitope repair. The tissue sections were rinsed in PBS. Tissue sections were blocked with 3% bovine serum albumin (BSA) for 30 min at room temperature. Then, the tissue sections were incubated with primary antibodies MGMT (1:100; Proteintech), Ki67 (1:500; Servicebio, Wuhan, China), and cleaved caspase-3 (1:500; Servicebio) overnight at 4 °C. Tissue sections were washed three times with PBS and incubated with biotinylated secondary antibodies for 30 min at room temperature. The tissue was washed three times with PBS and incubated with streptavidin-biotin-peroxidase complex for 20 min at room temperature after incubation of the secondary antibody. Sections were stained using diaminobenzidine (DAB). Finally, the nuclei were stained with hematoxylin, and then the sections were dehydrated, sealed, and microscopically observed.

Table 2
Short hairpin RNA (ShRNA) sequences.

ShRNA names	Sequences
shMGMT-SiR1+	5′-ccggCAAGGATTGTGAAATGAAAggatccTTTCATTTCA CAATCCTTGttttttg-3′
shMGMT-SiR1−	5′-aattcaaaaaCAAGGATTGTGAAATGAAAggatccTTTCATT TCACAATCCTTG-3′
shMGMT-SiR2+	5′-ccggGACAAGGATTGTGAAATGAggatccTCATTTCACA ATCCTTGTCttttttg-3′
shMGMT-SiR2−	5′-aattcaaaaaGACAAGGATTGTGAAATGAggatccTCATTT CACAATCCTTGTC-3′
shMGMT-SiR3+	5′-ccggGTTCACCAGACAGGTGTTAggatccTAACACCTGT CTGGTGAACttttttg-3′
shMGMT-SiR3−	5′-aattcaaaaaGTTCACCAGACAGGTGTTAggatccTAACAC CTGTCTGGTGAAC -3′
shCTNNB1-SiR1+	5′-ccggGGGTTCAGATGATATAAATggatccATTTATATCAT CTGAACCCttttttg-3′
shCTNNB1-SiR1−	5′-aattcaaaaaGGGTTCAGATGATATAAATggatccATTTATAT CATCTGAACCC-3′
shCTNNB1-SiR2+	5′-ccggCCCAAGCTTTAGTAAATATggatccATATTTACTAA AGCTTGGGttttttg-3′
shCTNNB1-SiR2−	5′-aattcaaaaaCCCAAGCTTTAGTAAATATggatccATATTTAC TAAAGCTTGGG-3′
shCTNNB1-SiR3+	5′-ccggGCCACAAGATTACAAGAAAggatccTTTCTTGTAA TCTTGTGGCttttttg-3′
shCTNNB1-SiR3−	5′-attcaaaaaGCCACAAGATTACAAGAAAggatccTTTCTTG TAATCTTGTGGC-3′
shXRCC6-SiR1+	5′-ccggCAGGGTGGGAGTCATATTAggatccTAATATGACT CCCACCCTGttttttg-3′
shXRCC6-SiR1−	5′-aattcaaaaaCAGGGTGGGAGTCATATTAggatccTAATATG ACTCCCACCCTG-3′
shXRCC6-SiR2+	5′-ccggGGTTGAAGCAATGAATAAAggatccTTTATTCATT GCTTCAACCttttttg-3′
shXRCC6-SiR2−	5′-aattcaaaaaGGTTGAAGCAATGAATAAAggatccTTTATTC ATTGCTTCAACC-3′

MGMT: O^6-methylguanine (O^6-MG)-DNA-methyltransferase.

2.15. TdT-mediated dUTP nick-end labeling (TUNEL) assay

C57BL/6J mice subcutaneous tumor sections were dewaxed and hydrated. Histochemical pens were used to draw circles on the tissue. The sample area was fixed using 4% paraformaldehyde for 15 min, and then the sample area was permeabilized with 20 μg/mL proteinase K at room temperature for 30 min. The sections were rinsed twice with PBS and excess liquid was blotted off using a filter paper. TUNEL reaction solution was prepared for staining according to the manufacturer's instructions for the TUNEL Apoptosis Kit (UElandy). After adding a 50 μL of TUNEL reaction solution to each sample area, the samples were incubated at 37 °C for 2 h. The TUNEL reaction solution was then discarded from the samples, and the samples were rinsed twice using PBS. The sample area was incubated with 5 μg/mL DAPI staining solution for 5 min at room temperature. After washing the sample area twice with PBS, excess liquid was blotted off with a filter paper, and 100 μL of PBS was added to the sample area to maintain moisture. Sections were observed using a fluorescent microscope (Nikon).

2.16. Immunofluorescence staining

Cells were fixed with 4% formaldehyde for 15 min and blocked with a mixture of PBS, 1% BSA, and 0.1% Triton X-100 for 2 h. Cells were incubated with anti-phospho-H2A.X (S139) rabbit pAb (1:200; Servicebio) at 4 °C overnight. Cells were washed three times with PBS and incubated with CoraLite488-conjugated goat anti-rabbit IgG (1:250; Proteintech) for 2 h at room temperature. The cells were washed three times with PBS. Finally, DAPI was used to stain the nucleus. Images were examined under a fluorescent microscope (Nikon).

2.17. Mass spectrometric analysis

HCT116 cells with MGMT-HA overexpression were lysed with a lysis buffer (20-mM Tris, 150-mM NaCl, and 1% Triton X-100; pH 7.5). HA tag polyclonal antibody (51064-2-AP; Proteintech) and rabbit IgG control polyclonal antibody (30000-0-AP; Proteintech) were incubated with lysis for 1 h at room temperature. Protein A/G Magnetic Beads (Epizyme, Inc., Shanghai, China) were washed with a binding buffer (50-mM Tris, 150-mM NaCl, and 0.1%–0.5% NP40; pH7.5). The antigen–antibody complexes were incubated with the beads for 1 h at room temperature. The antigen–antibody–beads complexes were washed with the binding buffer, and mass spectrometry (MS) analysis was conducted. The identified proteins were enriched through the Kyoto Encyclopedia of Genes and Genomes (KEGG) pathway using Sangerbox 3.0 software.

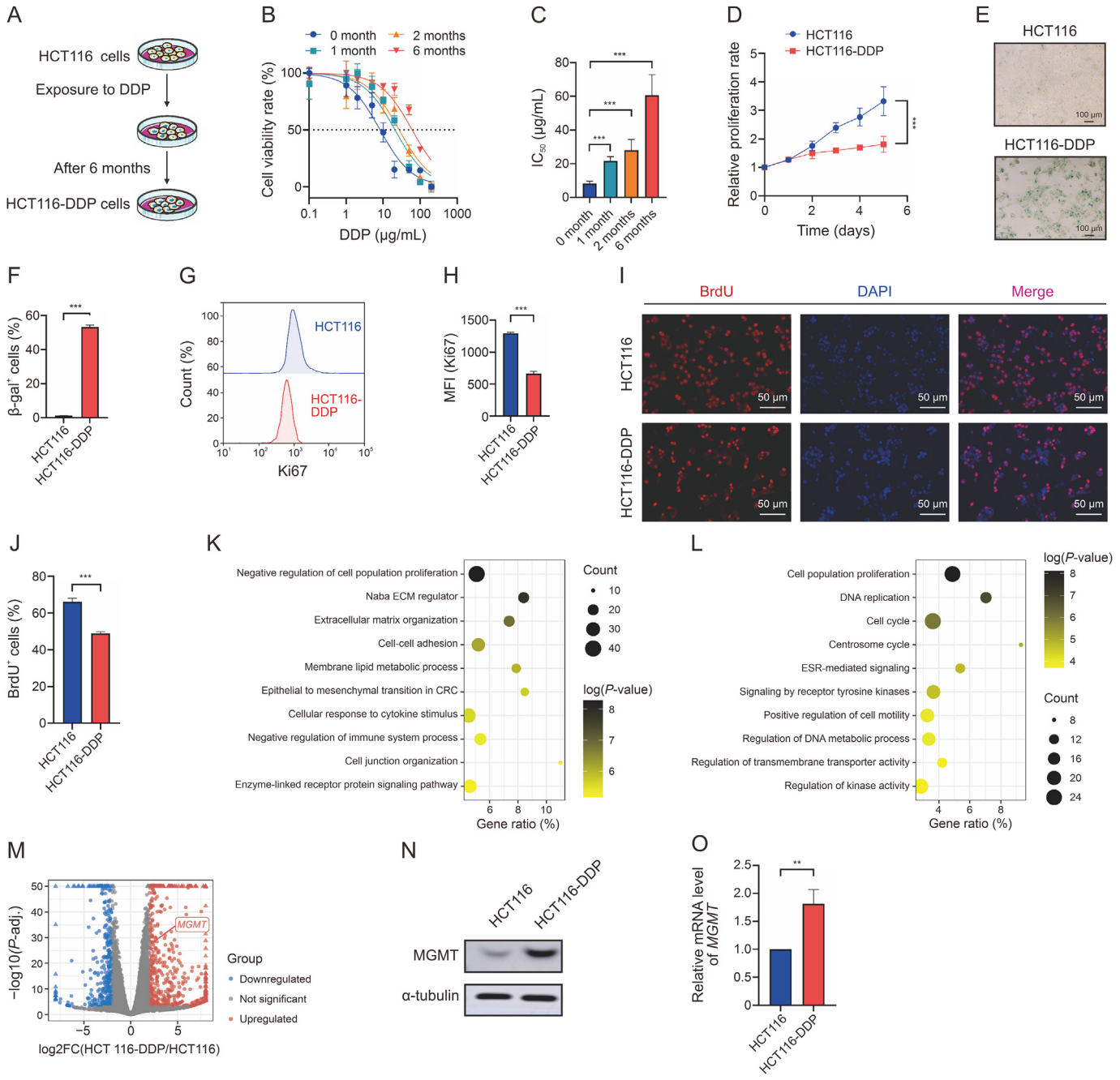

Fig. 1. Elevated O^6-methylguanine (O^6-MG)-DNA methyltransferase (MGMT) expression is related to slow-cycling cells and DNA damage repair in cisplatin (DDP)-resistant colorectal cell line. (A) Culture of DDP-resistant cell lines. (B, C) Half maximal inhibitory concentration (IC_{50}) curves (B) and IC_{50} values (C) of HCT116-DDP cells to DDP at 0, 1, 2, and 6 months. (D) Proliferation of HCT116 and HCT116-DDP cells. (E) Representative images of β-galactosidase (β-gal) staining in HCT116 and HCT116-DDP cells. (F) Percentage of β-gal positive cells in HCT116 and HCT116-DDP cells. (G) Ki67 staining intensity of HCT116 and HCT116-DDP cells by flow cytometry. (H) Quantification of Ki67 expression in HCT116 and HCT116-DDP cells. (I) 5-Bromo-2′-deoxyuridine (BrdU) staining for HCT116 and HCT116-DDP cells. (J) Proportion of BrdU-positive cells in HCT116 and HCT116-DDP cells. (K, L) Gene Ontology (GO) enrichment analysis of upregulated (K) and downregulated (L) genes in HCT116-DDP compared to HCT116. (M) Volcano map analysis for altered genes in HCT116-DDP compared to HCT116. (N) Protein level expression of MGMT in HCT116 and HCT116-DDP. (O) Messenger RNA (mRNA) level expression of MGMT in HCT116 and HCT116-DDP. Data were statistically analyzed using Student's *t*-test. $^{**}P < 0.01$ and $^{***}P < 0.001$. ns: no significance. MFI: mean fluorescence intensity; DAPI: 4,6-diamino-2-phenyl indole; ECM: extracellular matrixc; CRC: colorectal cancer; ESR: erythrocyte sedimentation rate.

2.18. Co-immunoprecipitation (Co-IP) assay

HCT116 cells and HCT116 cells with MGMT-HA overexpression were lysed using 500 μL of a binding buffer (50 mM Tris, 150 mM NaCl, and 0.1%–0.5% NP40; pH7.5) with the addition of phenylmethanesulfonyl fluoride. Approximately 25 μL of anti-HA magnetic beads (Epizyme) was washed with a binding buffer. The lysis was incubated with the beads for 1 h at room temperature. The antigen–antibody–beads complexes were washed with a binding buffer, and then a 50 μL of 1× SDS-PAGE loading buffer was added to the tube. The tubes were heated and boiled at 100 °C for 10 min. To detect CDK1 (ET1607-51; Huabio, Hangzhou, China), XRCC6

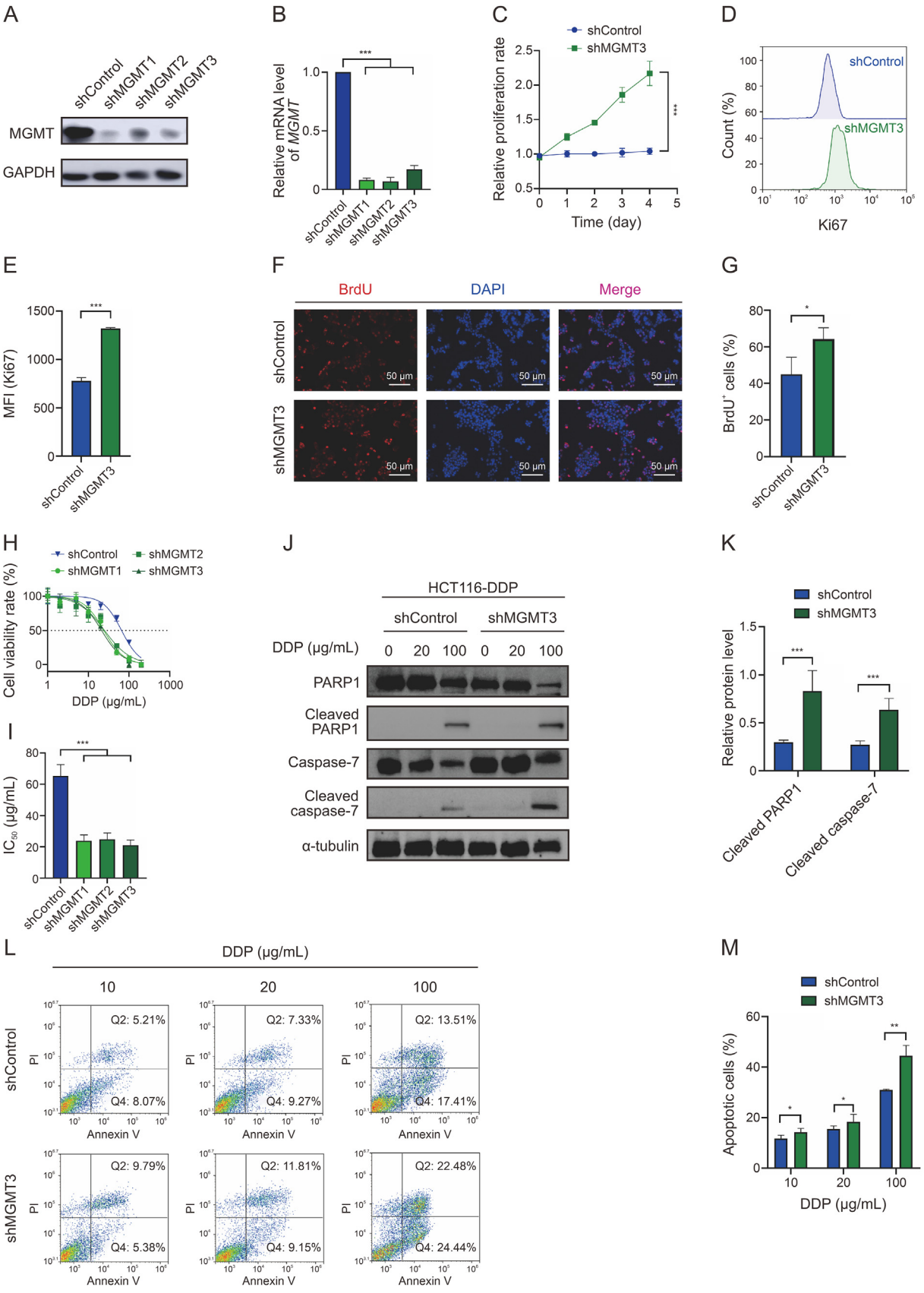

Fig. 2. Knockdown of O^6-methylguanine (O^6-MG)-DNA methyltransferase (MGMT) enhances cisplatin (DDP) susceptibility in HCT116-DDP cells. (A) MGMT expression level in HCT116-DDP cells with MGMT knockdown by Western blot assay. (B) Messenger RNA (mRNA) level expression of MGMT in HCT116-DDP cells with MGMT knockdown. (C) Proliferation of HCT116-DDP cells with or without MGMT knockdown. (D) Ki67 staining intensity of HCT116-DDP with or without MGMT knockdown by flow cytometry. (E) Quantification of Ki67 expression in HCT116-DDP cells with or without MGMT knockdown. (F) 5-Bromo-2′-deoxyuridine (BrdU) staining of HCT116-DDP cells with or without MGMT

(66607-1-Ig; Proteintech), and HA tag (51064-2-AP; Proteintech) expression, Western blotting was performed. The same method was employed to SW480 cells to detect the interaction.

2.19. Mouse subcutaneous tumor model

Male C57BL/6J mice (6–8 weeks old, 18–20 g) were obtained from the experimental animal center of Xi'an Jiaotong University (Xi'an, China). Animals were housed under standard specific pathogen-free conditions with standard chow and typical light/dark cycle. The mice were allowed seven days to adapt to the environment prior to the experiment.

Vector MC38 cells and MGMT-overexpression (OE) MC38 cells (1×10^6/mouse) were subcutaneously injected into the right back of C57BL/6J mice. When the tumor volume reached 50–100 mm^3, treatment was initiated. Mice bearing vector MC38 cells were then injected with DDP (4 mg/kg; TopScience, Shanghai, China) intraperitoneally every three days as a control group. Mice bearing MGMT-OE MC38 cells were randomly divided into two groups ($n = 5$/group). The mice in the MGMT-OE + DDP group were then treated with DDP every three days, and mice in the MGMT-OE + DDP + O^6-benzylguanine (O^6-BG) group were treated with DDP and O^6-BG (5 mg/kg; Topscience) every three days.

The weight and tumor sizes were measured every two days after administration and calculated using a caliper expressed using the following formula: $1/2 \times \text{length} \times \text{width}^2$. The mice in each group were sacrificed to dissect the tumor and the tumor weight was recorded on day 20. All animal procedures were conducted in accordance with ethical regulations for animal testing and research and were approved by the Medical Ethics Committee of Xi'an Jiaotong University (Approval No.: 2023-22).

2.20. Statistical analysis

All data were presented as the means ± standard deviation (SD), and statistical analyses were performed using the GraphPad Prism (version 8, La Jolla, CA, USA) with Student's *t*-test. For all analyses, statistical significance was set at $P < 0.05$.

3. Results

3.1. Cisplatin (DDP)-resistant colorectal cell line demonstrated an elevated level of MGMT expression

HCT116 cells were exposed to the complete medium with DDP for a long time, and DDP-resistant cells were obtained after 6 months (Fig. 1A). The IC_{50} for DDP in the DDP-resistant cell lines was eight-fold higher than that of the parental cells (Figs. 1B and C). Meanwhile, the DDP-resistant cell lines also demonstrated resistance to oxaliplatin (Figs. S1A and B), indicating the presence of multidrug resistance in DDP-resistant cells. Phospho-H2A.X (S139) (γ-H2AX) staining revealed that DDP-resistant cells were more resistant to DDP-induced DSBs than parental cells (Figs. S1C and D). Growth curves were plotted via the MTT assay, indicating that HCT116-DDP grew significantly slower than the parental cells (Fig. 1D). β-gal staining revealed a significantly higher senescence rate of HCT116-DDP than that of the parental cells (Figs. 1E and F), accompanied by remarkable slow growth features. The mean fluorescence intensity (MFI) of Ki67 was significantly decreased in HCT116-DDP compared to the parental cells through flow cytometry analysis (Figs. 1G and H). Meanwhile, the proportion of BrdU-positive cells in HCT116-DDP cells was considerably reduced than that of parental cells (Figs. 1I and J), which is consistent with β-gal and Ki67 staining. The above results indicated that drug-resistant cells escape from chemotherapy through a temporary reduction of proliferation.

We performed transcriptome sequencing on drug-resistant cells and parental cells to explore the mechanism of DDP-induced resistance in CRC. Gene Ontology (GO) analysis suggested that the genes with an elevated expression were mainly enriched in the negative regulation of the cell population proliferation pathway (Fig. 1K), while the downregulated genes were mostly enriched in cell proliferation, DNA replication, and cell cycle pathway (Fig. 1L). MGMT was noted among the elevated genes through gene expression difference analysis (Fig. 1M). MGMT is involved in the DNA-repair system that can remove alkylating lesions using DNA alkyltransferase such as DDP. To validate the expression level of MGMT in parental cells and HCT116-DDP, which revealed that MGMT was significantly elevated in HCT116-DDP, immunoblotting (Fig. 1N) and qPCR (Fig. 1O) were employed. Additionally, we used the Search Tool for Recurring Instances of Neighbouring Genes (STRING) database for interaction analysis (Figs. S1E and F) to explore the relationship between MGMT and the relevant enrichment pathways, which showed a close relationship between MGMT and DNA replication and cell cycle pathways. These results indicate that cell proliferation repression and DNA damage repair are closely related to DDP-induced drug resistance with MGMT being involved.

3.2. Repression of MGMT restores drug-resistant cell sensitivity to DDP

We knocked down MGMT in HCT116-DDP and tested its efficiency to examine the role of MGMT in DDP-resistant cells (Figs. 2A and B). The MGMT knockdown accelerates the cell growth rate through the MTT assay (Fig. 2C). The promotion of proliferation was further verified by Ki67 staining (Figs. 2D and E) and BrdU staining (Figs. 2F and G) in HCT116-DDP cells after MGMT knockdown. Moreover, the IC_{50} of the HCT116-DDP cells with MGMT knockdown to DDP and oxaliplatin were significantly decreased (Figs. 2H, 2I, S2A, and S2B), suggesting that MGMT mediates chemoresistance in CRC. We examined the expression of pro-apoptotic markers (PARP1, cleaved PARP1, caspase-7, and cleaved caspase-7) after DDP treatment to investigate the mechanism (Fig. 2J). The accumulation of cleaved PARP1 and cleaved caspase-7 in drug-resistant cells was noted after elimination of MGMT after 100 μg/mL DDP treatment (Fig. 2K), and the apoptosis rate of HCT116-DDP under DDP treatment after MGMT knockdown was elevated (Fig. 2L). The apoptosis rate was demonstrated in a dose-dependent manner and markedly increased after MGMT depletion (Fig. 2M). γ-H2AX staining revealed that MGMT knockdown could enhance DSBs induced by DDP (Figs. S2C and D). To further test targeting MGMT to restore DDP sensitivity in drug-resistant cells, we applied O^6-BG, a potent MGMT inhibitor, combined with DDP on drug-resistant cells. HCT116-DDP was found to be more sensitive to O^6-BG with a slightly lower IC_{50} compared to the parental cells (Figs. S2E and F).

knockdown. (G) Proportion of BrdU-positive cells in HCT116-DDP cells with or without MGMT knockdown. (H, I) Half maximal inhibitory concentration (IC_{50}) curves (H) and values (I) in HCT116-DDP cells with or without MGMT knockdown to DDP. (J) The expression levels of poly (adenosine diphosphate (ADP)-ribose) polymerase 1 (PARP1), cleaved PARP1, caspase-7, and cleaved caspase-7 in HCT116-DDP cells with or without MGMT knockdown after treatment with DDP. (K) Quantification of cleaved PARP1 and cleaved caspase-7 in HCT116-DDP cells with or without MGMT knockdown by 100 μg/mL DDP. (L) Apoptosis levels in HCT116-DDP with or without MGMT knockdown after treatment with DDP by flow cytometry analysis. (M) Quantitative analysis of apoptosis rate of HCT116-DDP cells with or without MGMT knockdown treated with 10, 20, and 100 μg/mL DDP. Data were statistically analyzed using Student's *t*-test. $^{*}P < 0.05$, $^{**}P < 0.01$, and $^{***}P < 0.001$. ns: no significance. GAPDH: glyceraldehyde-3-phosphate dehydrogenase; sh: short hairpin; MFI: mean fluorescence intensity; DAPI: 4,6-diamino-2-phenyl indole; PI: propidium iodide.

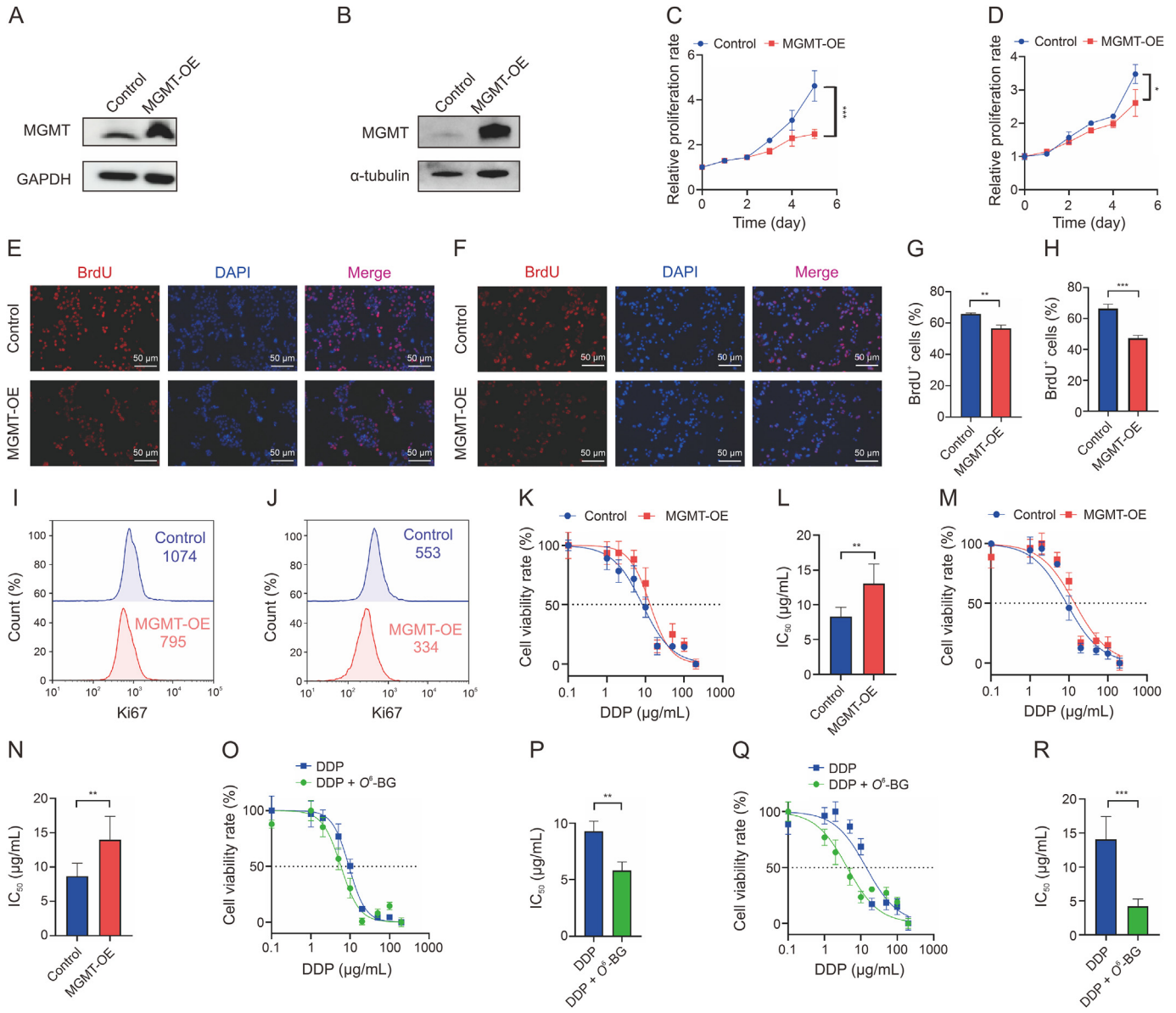

Fig. 3. Overexpression of O^6-methylguanine (O^6-MG)-DNA methyltransferase (MGMT) decreases the cisplatin (DDP) sensitivity in colorectal cell lines. (A, B) The expression levels of MGMT in HCT116 (A) and SW480 (B) with or without MGMT overexpression. (C, D) Proliferation of HCT116 (C) and SW480 (D) with or without MGMT overexpression. (E, F) 5-Bromo-2′-deoxyuridine (BrdU) stainings of HCT116 (E) and SW480 (F) cells with or without MGMT overexpression. (G, H) Proportion of BrdU-positive cells in HCT116 (G) and SW480 (H) cells with or without MGMT overexpression. (I, J) Ki67 stain intensity of HCT116 (I) and SW480 (J) cells with or without MGMT overexpression by flow cytometry. (K, L) Half maximal inhibitory concentration (IC_{50}) curves (K) and values (L) of DDP on HCT116 with or without MGMT overexpression. (M, N) IC_{50} curves (M) and values (N) of DDP on SW480 with or without MGMT overexpression. (O, P) IC_{50} curves (O) and values (P) of DDP on HCT116 cells overexpressing MGMT with or without O^6-benzylguanine (O^6-BG) (50 μM). (Q, R) IC_{50} curves (Q) and values (R) of DDP on SW480 overexpressing MGMT with or without O^6-BG (50 μM). Data were statistically analyzed using the Student's *t*-test. $^*P < 0.05$, $^{**}P < 0.01$, and $^{***}P < 0.001$. ns: no significance. OE: overexpression; DAPI: 4,6-diamino-2-phenyl indole.

However, IC_{50} to DDP was significantly decreased when combined with 50 μM O^6-BG compared to the control group (Figs. S2G and H). These results support that the MGMT expression level is positively correlated with resistance of CRC cells to DDP.

3.3. *MGMT overexpression is associated with DDP resistance by inducing slow-cycling cells*

We stably overexpressed MGMT in HCT116 and SW480 to further elucidate the role of MGMT in CRC cells. MGMT expression level was significantly elevated in the overexpression group through an immunoblotting assay (Figs. 3A and B). The cancer cell proliferation rate was repressed after MGMT overexpression (Figs. 3C and D), which was supported by less BrdU incorporation (Figs. 3E–H) and the decline in Ki67 (Figs. 3I and J). Meanwhile, the IC_{50} of the MGMT overexpression groups to DDP was significantly increased (Figs. 3K–N) indicating that it was less sensitive compared to the control. Consistently, MGMT overexpression has been shown to significantly enhance CRC cell resistance to oxaliplatin (Figs. S3A–D). O^6-BG could partially reverse MGMT-mediated anti-apoptosis to DDP treatment. Consistently, IC_{50} for DDP significantly decreased in the combination group (DDP + O^6-BG) compared to DDP alone (Figs. 3O–R). Thus, O^6-BG inhibited DDP resistance caused by MGMT.

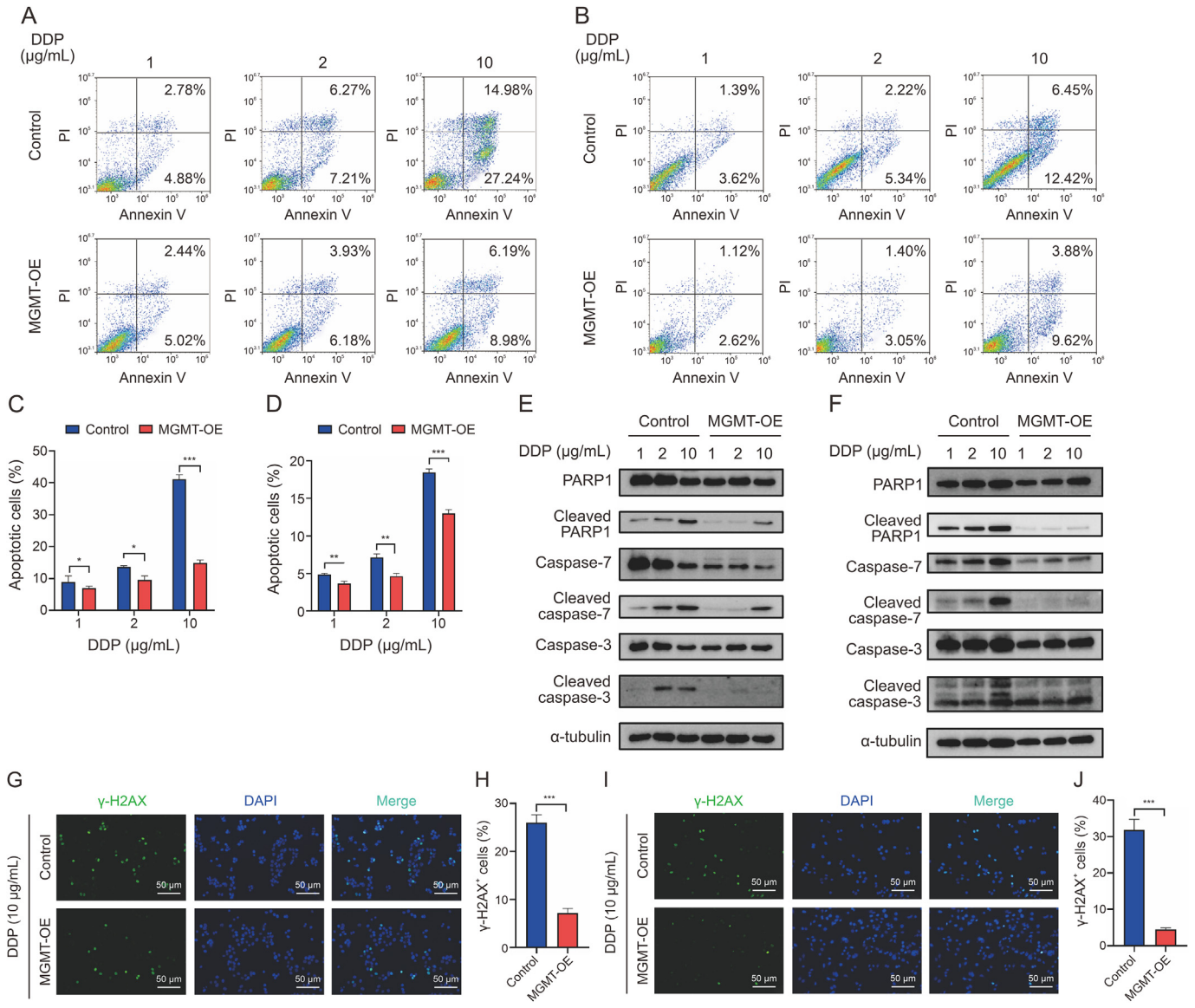

Fig. 4. O^6-methylguanine (O^6-MG)-DNA methyltransferase (MGMT) overexpression enhances cisplatin (DDP)-induced apoptosis in HCT116 and SW480 cells. (A, B) Apoptosis levels in HCT116 (A) and SW480 (B) cells with or without MGMT overexpression after treatment with DDP by flow cytometry analysis. (C) Quantitative analyses of apoptosis rates of HCT116 (C) and SW480 (D) cells with or without MGMT overexpression treated with 1, 2, and 10 μg/mL DDP. (E, F) The expression levels of HCT116 (E) and SW480 (F) with or without MGMT overexpression apoptosis markers poly (adenosine diphosphate (ADP)-ribose) polymerase 1 (PARP1), cleaved PARP1, caspase-3, cleaved caspase-3, caspase-7, and cleaved caspase-7 after treatment with DDP. (G) Phospho-H2A.X (S139) (γ-H2AX) staining for HCT116 cells with or without MGMT overexpression after DDP treatment. (H) Percentage of γ-H2AX positive cells in HCT116 cells with or without MGMT knockdown after DDP treatment. (I) γ-H2AX staining for SW480 cells with or without MGMT overexpression after DDP treatment. (J) Percentage of γ-H2AX positive cells in SW480 cells with or without MGMT knockdown after DDP treatment. Data were statistically analyzed using Student's *t*-test. $^{*}P < 0.05$, $^{**}P < 0.01$, and $^{***}P < 0.001$. ns: no significance. OE: overexpression; PI: propidium iodide; DAPI: 4,6-diamino-2-phenyl indole.

3.4. MGMT overexpression alleviated DDP-induced apoptosis and DSBs

After DDP treatment, the apoptosis rates of the MGMT overexpression groups were significantly lower than that of the control group (Figs. 4A–D). The accumulation of cleaved PARP1, cleaved caspase-3, and cleaved caspase-7 were accompanied by an increase in DDP concentration; however, the expression levels dramatically declined in the overexpression group (Figs. 4E and F). γ-H2AX staining showed that MGMT overexpression weakened DDP-induced DSBs in HCT116 (Figs. 4G and H) and SW480 (Figs. 4I and J) cells. In conclusion, we found that MGMT overexpression in CRC cells promoted DDP treatment resistance.

3.5. MGMT overexpression drives DDP resistance in vivo which can be restored via O^6-BG

MGMT was overexpressed in murine-derived colon cancer cell MC38 followed by subcutaneous injection into the C57BL/6J mice (Figs. 5A and B). The mice were divided into three groups: Vector + DDP, MGMT-OE + DDP, and MGMT-OE + DDP + O^6-BG groups. Treatment was initiated on day 8 after subcutaneous injection of tumor cells, and DDP (4 mg/kg) alone or combined with O^6-BG (5 mg/kg) was injected intraperitoneally every three days, respectively. No significant differences were found for the body weight among the three groups of mice, and the tumor grew faster in the MGMT-OE + DDP group compared to the Vector + DDP

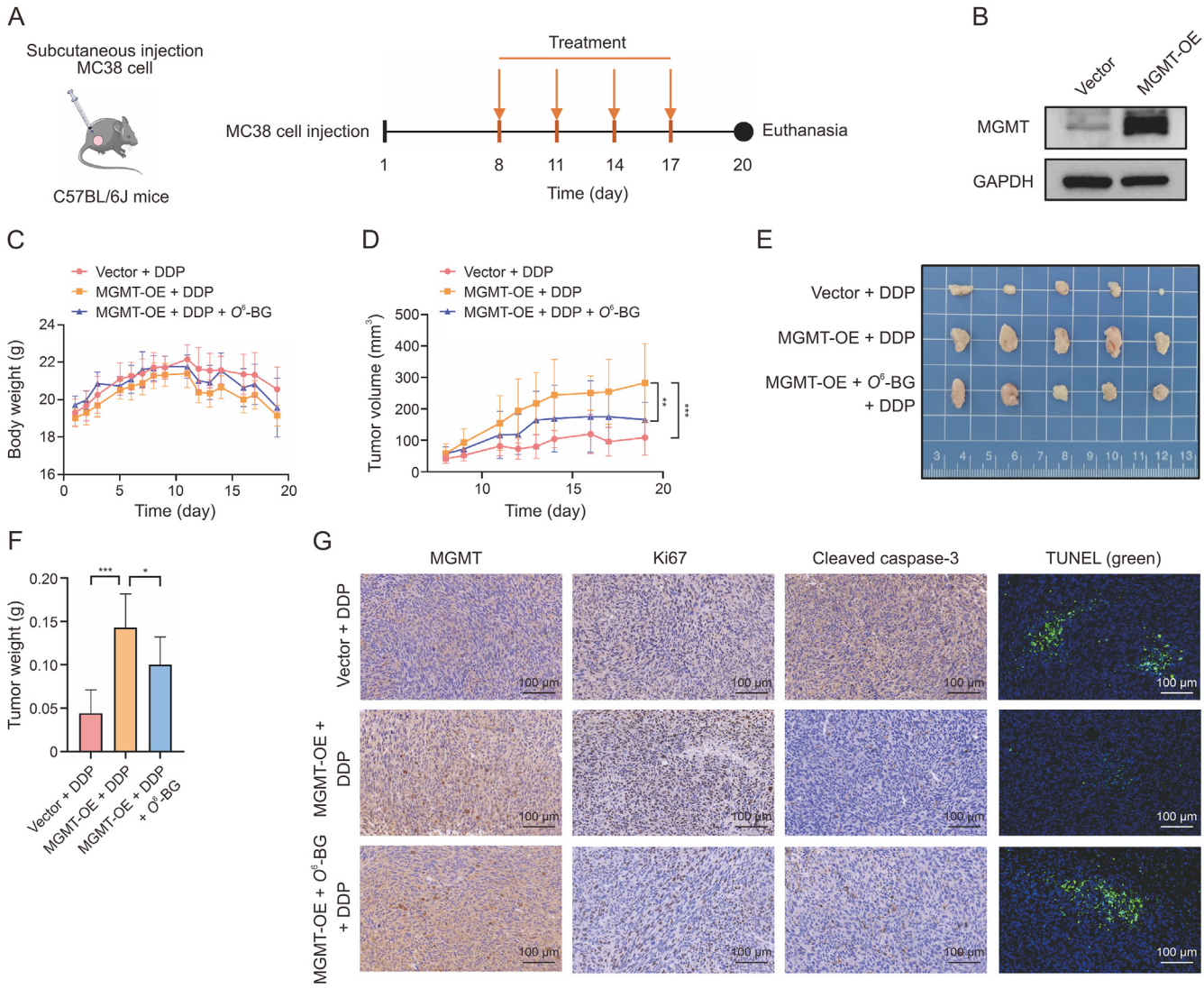

Fig. 5. *In vivo* validation of O^6-methylguanine (O^6-MG)-DNA methyltransferase (MGMT) affects the sensitivity of cisplatin (DDP) treatment. (A) Construction and treatment of subcutaneous tumors in C57BL/6J mice. MC38 cells transfected with vector or MGMT were inoculated into C57BL/6J mice. DDP was injected at 4 mg/kg every three days. In the MGMT-overexpression (OE) + O^6-benzylguanine (O^6-BG) + DDP group, O^6-BG was injected at 5 mg/kg in parallel with DDP. After four cycles, tumors were harvested to measure their size and weight. (B) The expression levels of MGMT in MC38 with or without MGMT overexpression. (C, D) Changes in body weight (C) and tumor volume (D) of the three groups of mice. (E, F) Tumor size (E) and tumor weight (F) of the three groups of mice. (G) Representative images are shown for immunohistochemistry (IHC) analysis of MGMT, Ki67, and cleaved caspase-3 and TdT-mediated dUTP nick-end labeling (TUNEL) fluorescence staining of tumor sections. Data were statistically analyzed using Student's *t*-test. $^{*}P < 0.05$, $^{**}P < 0.01$, and $^{***}P < 0.001$. ns: no significance.

group, which was partially reduced in the MGMT-OE + DDP + O^6-BG group (Figs. 5C and D). All mice were sacrificed after 20 days, and subcutaneous tumors were obtained (Figs. 5E and F). Under treatment, Ki67 expression was significantly upregulated in the MGMT-OE + DDP group compared to the Vector + DDP group, and cleaved caspase-3 expression was significantly weakened together with a decreased TUNEL stain intensity. The MGMT-OE + O^6-BG + DDP group demonstrated a lower Ki67 expression, cleaved caspase-3 accumulation, and higher TUNEL stain intensity compared to the MGMT-OE + DDP group (Fig. 5G). Altogether, MGMT mediated DDP-induced resistance *in vivo* and can be partially reversed via O^6-BG.

3.6. MGMT induces slow-cycling cells by degrading CDK1

We analyzed the expression of cell cycle-related proteins (P21, P16, CDK1, and cyclin D1) in HCT116-DDP cells after MGMT knockdown to investigate the mechanism of how MGMT affects cell proliferation (Fig. 6A). P21 and P16 decreased, while the CDK1 expression increased after MGMT depletion. Meanwhile, P21 and P16 were upregulated and cyclin D1 and CDK1 were reduced in MGMT-overexpressed HCT116 cells (Fig. 6B). p21 was upregulated and CDK1 and cyclin D1 were reduced in MGMT-overexpressed SW480 cells; however, p16 did not significantly change (Fig. 6C). Since P21 and CDK1 were consistent in resistant cells and parental cells, we highlighted on P21 and CDK1, which have been reported as major regulators of the cell cycle.

To determine how MGMT affects the cell cycle, we stably overexpressed MGMT-HA in HCT116 cells. The HA immunomagnetic beads were used for immunoprecipitation, and the precipitated antigen–antibody complex was analyzed using protein MS, with the IgG magnetic beads as control (Fig. 6D). The IgG and HA groups were then analyzed using a Venn diagram, and 522 proteins were screened (Fig. 6E). Using the KEGG database, these proteins were enriched. Pathways such as base excision repair, DNA replication, cell cycle, and nonhomologous end joining were identified (Fig. 6F).

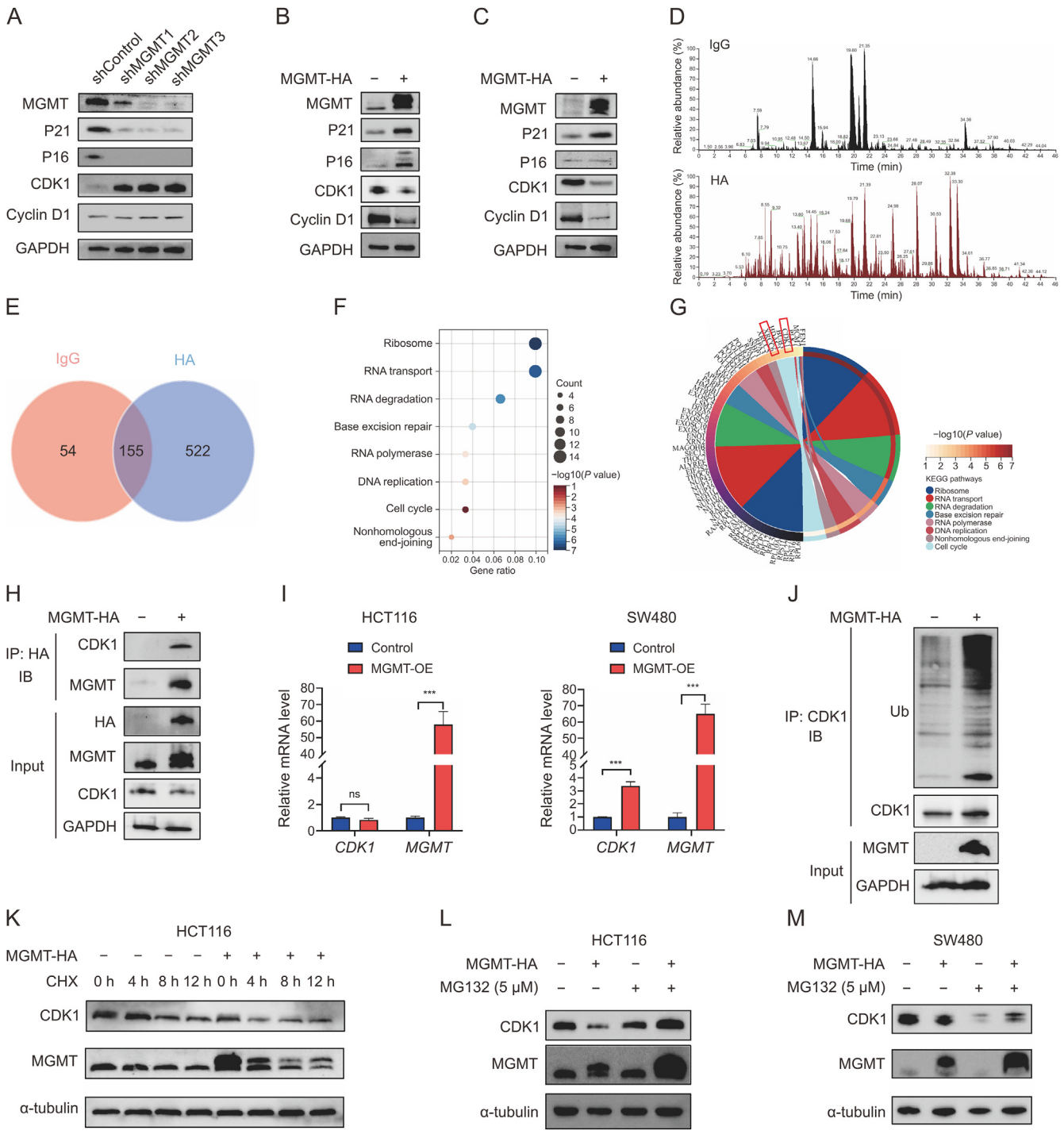

Fig. 6. O^6-methylguanine (O^6-MG)-DNA methyltransferase (MGMT) induces slow cycling cells by promoting ubiquitination mediated degradation of cyclin dependent kinase 1 (CDK1). (A) Protein expression of cell cycle markers cyclin dependent kinase inhibitor 2A (P16), cyclin dependent kinase inhibitor 1A (P21), CDK1, and cyclin D1 in HCT116-cisplatin (DDP) with or without MGMT knockdown. (B, C) Protein expression of cell cycle markers P16, P21, CDK1, and cyclin D1 in HCT116 (B) and SW480 (C) cells with or without MGMT overexpression. (D) Mass spectrometry (MS) analysis of proteins interacting with MGMT. (E) Venn diagram analysis of MS results of HA group compared to IgG group. (F) Kyoto Encyclopedia of Genes and Genomes (KEGG) enrichment of proteins interacting with MGMT. (G) Proteins that interact with MGMT. (H) Co-Immunoprecipitation (Co-IP) of MGMT and CDK1 in HCT116 cells. (I) Messenger RNA (mRNA) expression level of CDK1 after MGMT overexpression in HCT116 and SW480 cells. (J) The ubiquitin level of CDK1 in HCT116 cells with or without MGMT overexpression. (K) CDK1 protein expression level in HCT116 cells with or without MGMT overexpression after cycloheximide (CHX) treatment. (L, M) CDK1 protein expression level in HCT116 (L) and SW480 (M) cells with or without MGMT overexpression after Z-Leu-Leu-Leu-al (MG132) treatment. Data were statistically analyzed using Student's *t*-test. $^{***}P < 0.001$. ns: no significance. sh: short hairpin; GAPDH: glyceraldehyde-3-phosphate dehydrogenase; IB: immunoblotting; Ub: ubiquitin.

We found CDK1 in the protein enriched by the cell cycle pathway and XRCC6 in the protein enriched in the NHEJ pathway (Fig. 6G). Moreover, the interaction between MGMT and CDK1 by Co-IP in HCT116 and SW480 cells was verified (Figs. 6H and S3E).

As the CDK1 mRNA level did not decrease in HCT116 and SW480 cells overexpressing MGMT (Fig. 6I), further investigation is warranted. We hypothesized that MGMT plays a vital role in the post-translational modification of CDK1. The ubiquitination level of

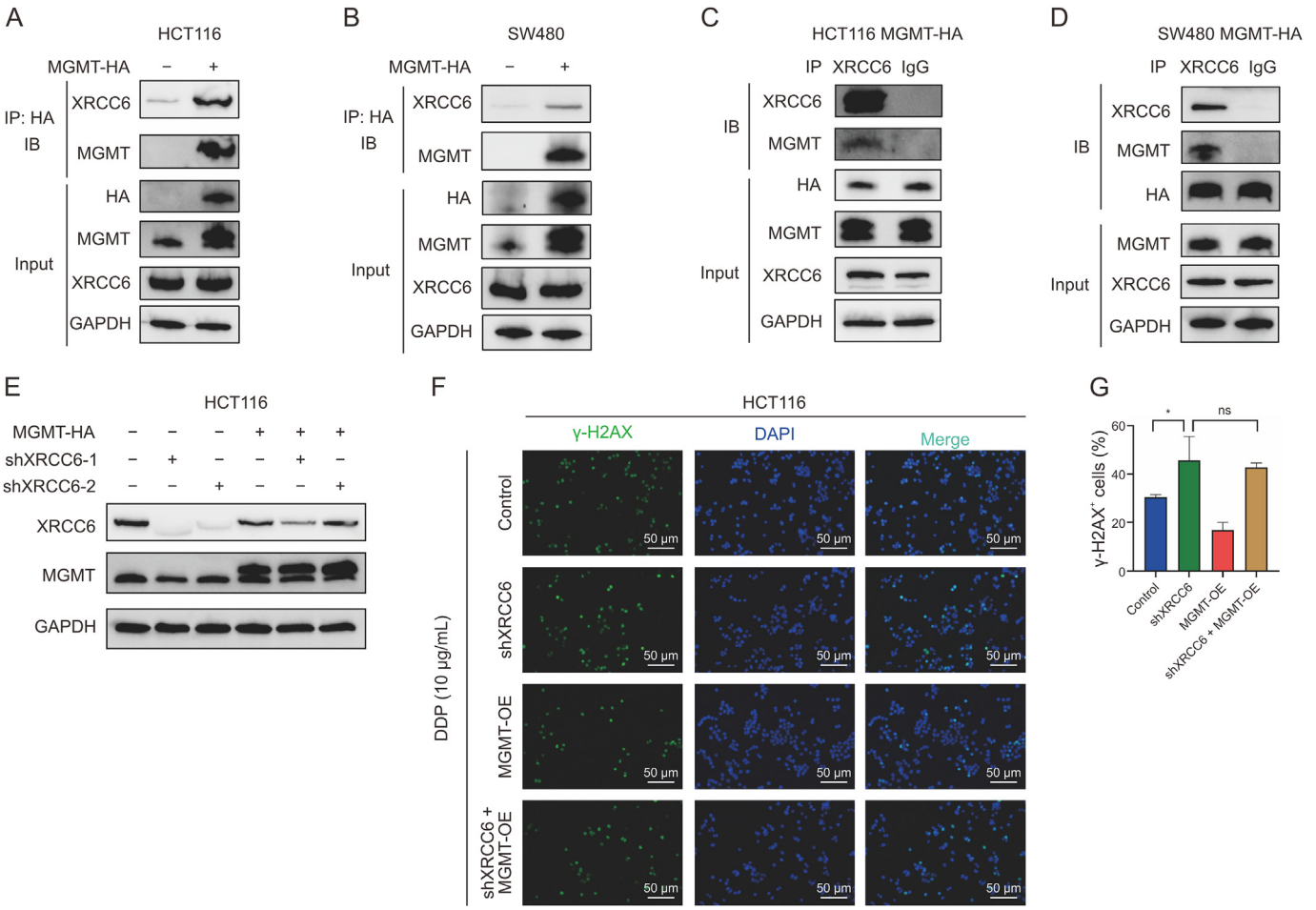

Fig. 7. O^6-methylguanine (O^6-MG)-DNA methyltransferase (MGMT) interacts with XRCC6 involved in the nonhomologous end joining. (A, B) Co-immunoprecipitation (Co-IP) of MGMT and XRCC6 in HCT116 (A) and SW480 (B) cells. (C, D) Reverse verification of the interaction between XRCC6 and MGMT in HCT116 (C) and SW480 (D) cells. (E) XRCC6 knockdown in HCT116 cells with or without MGMT overexpression. (F) Phospho-H2A.X (S139) (γ-H2AX) staining for HCT116 cells with or without XRCC6 knockdown and MGMT overexpression after cisplatin (DDP) treatment. (G) Percentage of γ-H2AX positive cells in HCT116 cells with or without XRCC6 knockdown and MGMT overexpression after DDP treatment. Data were statistically analyzed using Student's *t*-test. $^*P < 0.05$. ns: no significance. IB: immunoblotting; GAPDH: glyceraldehyde-3-phosphate dehydrogenase; sh: short hairpin; DAPI: 4,6-diamino-2-phenyl indole; OE: overexpression.

CDK1 was examined, and it was found that MGMT overexpression can significantly increase the CDK1 ubiquitination level (Fig. 6J). We exposed HCT116 cells with or without MGMT overexpression to cycloheximide (CHX) (10 mg/mL) every 4 h for 12 h. Compared to the control group, MGMT overexpression had a significant adverse effect on CDK1 (Fig. 6K). Thereafter, we exposed HCT116 and SW480 cells with or without MGMT overexpression to MG132 (5 μM). MG132 can significantly rescue CDK1 degradation caused by MGMT (Figs. 6L and M). The above results indicate that MGMT may mediate slow-cycling cell generation through ubiquitination degradation of CDK1.

3.7. MGMT interacts with XRCC6 for NHEJ to resist DNA damage induced by DDP

We screened XRCC6 according to the previous MS results to demonstrate the ability of MGMT to repair DSBs. NHEJ is a vital DNA-repair pathway that repairs DSBs and allows resistance to platinum-based chemotherapy such as DDP. The interaction between MGMT and XRCC6 through Co-IP was verified (Figs. 7A–D). To verify that MGMT achieves NHEJ through XRCC6, we knocked down XRCC6 in HCT116 cells with or without MGMT overexpression (Fig. 7E). We treated the cells with DDP and subsequently stained them with γ-H2AX. The results revealed that MGMT overexpression could significantly reduce DDP-induced DSBs. However, XRCC6 knockdown on the basis of MGMT overexpression can significantly increase DDP-induced DSBs (Figs. 7F and G). Furthermore, the EJ5-GFP plasmid was employed to establish the correlation between MGMT expression and NHEJ activity. The results demonstrated that MGMT overexpression can significantly enhance the occurrence of NHEJ (Figs. S3F and G). These findings highlight the significance of the MGMT-XRCC6 complex in the NHEJ pathway and its possible application for DDP-resistant cancer treatment.

3.8. MGMT confers drug-resistant cells via the Wnt pathway activation

To investigate the upstream factors of MGMT in DDP-resistant cancer cells, we treated HCT116-DDP cells with 58 inhibitors targeting the most frequently aberrantly activated pathways in CRC, including the Wnt/beta catenin, Hedgehog/smoothened, phosphoinositide 3-kinase/protein kinase B/mechanistic target of rapamycin (PI3K/Akt/mTOR), Notch, casein kinase, and CDKs, among others (Fig. 8A). All inhibitors were used at a concentration of 10 μM. Inhibitors are considered effective when the cell viability

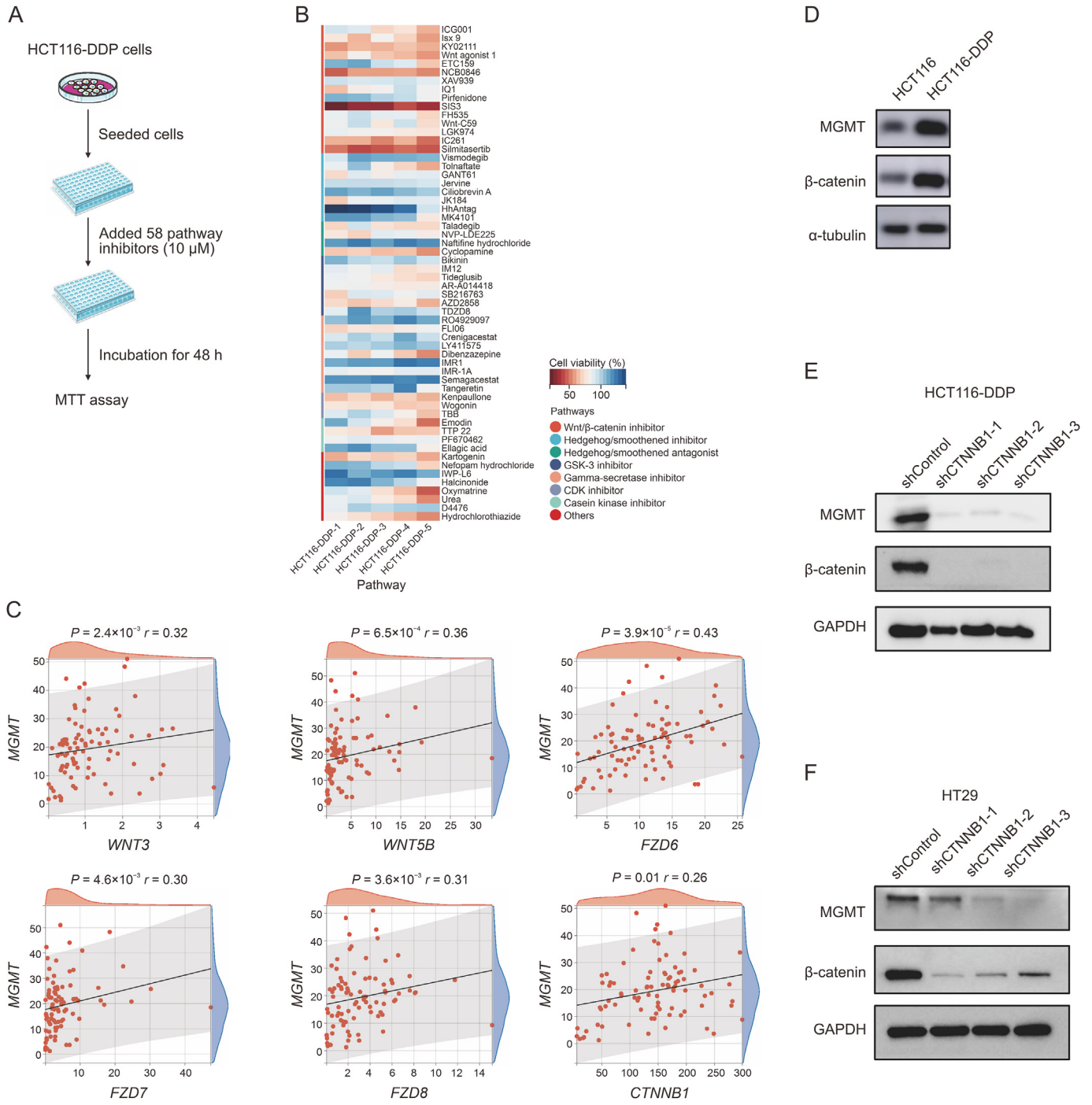

Fig. 8. Drug-resistant cells show a correlation between the activation of the Wnt pathway and elevated O^6-methylguanine (O^6-MG)-DNA methyltransferase (MGMT) levels. (A) Eight classes of pathway inhibitors (58 in total) were used on HCT116-cisplatin (DDP) for pathway screening. (B) Heat map showing the results of inhibitor screening of HCT116-DDP cells. (C) MGMT and Wnt pathway key factors correlation analysis by transcriptome data from 88 CRC patients' tissue. (D) Protein expression levels of MGMT and β-catenin in HCT116 and HCT116-DDP cells. (E, F) Expression levels of MGMT in HCT116-DDP (E) and HT29 (F) cells with or without β-catenin knockdown. MTT: thiazolyl blue tetrazolium bromide; GSK-3: glycogen synthase kinase-3; CDK: cyclin-dependent kinases.

is below 50%. Among them, Wnt/beta-catenin inhibitors demonstrated a pronounced inhibitory effect on drug-resistant cells (Fig. 8B). It was suggested that the Wnt signal cascade contributes to the acquired drug resistance in CRC cells. Furthermore, we performed a correlation analysis between key factors of the Wnt pathway (WNT3, WNT5B, FZD6, FZD7, FZD8, and CTNNB1) and MGMT by sequencing transcriptome data from 88 CRC patients' tumor tissues (Fig. 8C), and the results revealed a positive correlation between the above factors and MGMT. Additionally, β-catenin and MGMT were simultaneously elevated in drug-resistant cells (Fig. 8D). Knockdown of β-catenin by shRNA repressed MGMT expression in HCT116-DDP and HT29 cells (Figs. 8E and F). These results demonstrated the Wnt dependency of MGMT in DDP-induced drug-resistant cancer cells.

4. Discussion

MGMT is a DNA-repair protein that prevents the adverse biological effects of DNA damage caused by guanine O^6-alkylation. Guanine O^6-alkylation can cause DNA point mutations, chromosomal aberrations, recombination, and single-strand breaks and DSBs at the molecular level [33]. The accumulation of guanine O^6-alkylation can lead to malignant cell transformation, proto-oncogene activation, or apoptosis [34]. Thus, in normal cells, MGMT often plays a positive role, eliminating the effects of alkylating agents, maintaining cellular genomic stability, and avoiding cell malignancy or death [34]. However, in tumor cells, MGMT prevents cells from inhibition by alkylating agents, which is attributed to drug resistance; thus, it is important that the dual role of MGMT for cancer prevention and treatment is elucidated [35]. Platinum is a first-line drug for CRC chemotherapy; however, acquired resistance limits its therapeutic effect. In this study, we found that MGMT promotes DDP resistance in CRC cells and MGMT inhibition restores the sensitivity of drug-resistant cells to DDP.

Compared to the parental cells, MGMT was significantly elevated in DDP-resistant cells. Drug-resistant cell exhibit a disadvantage in growth rate compared to the parental cells, and transcriptome sequencing revealed that differentially expressed genes were enriched in cell proliferation regulation, DNA repair, and cell cycle pathways. The drug resistance could be attributed to slow-cycling state or DNA repair. Protein-protein interaction network analysis showed interactions between the MGMT and cell cycle as well as DNA-repair pathways. Hence, MGMT could impact drug resistance through cell cycle state alterations in addition to repairing DDP-induced DNA damage. To validate this hypothesis, we knocked down MGMT in drug-resistant cells and assessed their proliferation through Ki67 and BrdU stainings. Moreover, we examined the occurrence of DSBs with γ-H2AX staining. One of the main ways to repair DSBs is NHEJ. The results revealed that the proliferation rate of drug-resistant cells increased significantly after MGMT knockdown. Meanwhile, the apoptosis rate and the DSBs extent of drug-resistant cells with MGMT knockdown increased significantly after DDP treatment. Conversely, the proliferation rate decreased and the resistance to DDP increased significantly in parental cells after MGMT overexpression. Consistently, the apoptosis rate and the degree of DSBs decreased remarkably in CRC cells with MGMT overexpression after DDP treatment.

In addition to excluding the impact of the alkylating agent, we observed a particular function of MGMT in regulating the proliferation rate and NHEJ. We exerted considerable effort to elaborate the molecular mechanism underlying MGMT function. According to the protein spectra results, the proteins that interact with MGMT are primarily focused on base excision repair, cell cycle, and NHEJ. CDK1 plays a crucial role among the proteins related to the cell cycle. After overexpressing MGMT in CRC cells, a significant decrease in the protein level of CDK1 was observed, while the mRNA did not demonstrate a consistent trend. We have shown that MGMT promotes ubiquitination for the degradation of CDK1, leading to slow-cycling cell formation. MG132 can inhibit the protein degradation of CDK1 by MGMT. According to previous studies, MGMT does not have a role in NHEJ. We found that MGMT may interact with XRCC6 and contribute to NHEJ. When XRCC6 was knocked down in cells that overexpressed MGMT concurrently, the effect was restored to the level observed in wild-type cells. This explained how MGMT can reduce the level of DSBs after DDP exposure.

MGMT is mainly regulated epigenetically and its promoter methylation level tends to predict the therapeutic effect of temozolomide in glioma [36], while there is limited knowledge regarding the mechanisms of MGMT in CRC. Wnt activity is critical for intestinal stem cell homeostasis and crypt cells [37], and adenomatous polyposis coli (APC) mutations are commonly found in colonic epithelial cell transformation [38]. The APC mutation can repress β-catenin intracytoplasmic degradation, leading to β-catenin accumulation in the nucleus and sustained transcription of Wnt target genes [39]. We found that multiple Wnt pathway inhibitors could repress cell viability of drug-resistant cells through a screening process, indicating that the Wnt pathway has the potential to maintain drug-resistant cancer cells. A positive correlation was also found between MGMT and key factors in the Wnt pathway from CRC patient tumor tissues. When shRNA was used to knockdown β-catenin in drug-resistant cells, MGMT was subsequently reduced, suggesting that β-catenin has a regulatory effect on MGMT. However, further evidence is required to demonstrate the direct regulatory effect of β-catenin on MGMT.

The mechanism of regulation and functions of MGMT as a marker of predicting chemotherapy sensitivity in glioma has been well studied. However, its role in CRC remains largely unclear. Our study demonstrated that MGMT promotes DDP resistance in CRC, while MGMT inhibition alleviates the resistance. MGMT could be regulated by the Wnt pathway, and inhibition of the Wnt pathway decreases MGMT expression. We demonstrated that MGMT can induce slow-cycle cells through the interaction with CDK1, thereby preventing cancer cells from chemotherapy drugs. Meanwhile, we found that MGMT interacts with XRCC6 to allow NHEJ to resist chemotherapy drugs. In conclusion, MGMT could be a promising predictive marker in CRC chemotherapy.

5. Conclusion

Our results indicate that CRC cells with higher MGMT expression were resistant to DDP treatment. MGMT knockdown or inhibition sensitized CRC cells to DDP treatment, whereas MGMT overexpression resulted in resistance to DDP. Additionally, MGMT expression in CRC-resistant cells is positively correlated with key factors of the Wnt pathway, and MGMT-mediated DDP resistance is inextricably due to the CDK1 and XRCC6 interaction.

CRediT author statement

Haowei Zhang: Conceptualization, Validation, Writing - Original draft preparation; **Qixin Li:** Formal analysis; Writing - Reviewing and Editing; **Xiaolong Guo:** Validation; **Hong Wu:** Methodology; **Chenhao Hu:** Formal analysis; **Gaixia Liu:** Investigation; **Tianyu Yu:** Visualization; **Xiake Hu:** Conceptualization; **Quanpeng Qiu:** Data curation; **Gang Guo:** Resources; **Junjun She:** Supervision, Funding acquisition; **Yinnan Chen:** Conceptualization, Supervision, Resources, Funding acquisition.

Declaration of competing interest

The authors declare that there are no conflicts of interest.

Acknowledgments

This work was supported by grants from the National Natural Science Foundation of China (Grant Nos.: 82003807 and 82173394), the Shaanxi Province Science Foundation, China (Grant No.: 2023-GHZD-19), the Medical Foundation-Clinical Integration Program of Xi'an Jiaotong University, China (Grant No.: YXJLRH2022043), and the Xi'an Jiaotong University Free Exploration and Innovation-Teacher Project Foundation (Grant No.: xzy012023104). The Figures were partly generated using Servier Medical Art, provided by Servier and licensed under a Creative Commons Attribution 3.0 unported license.

Appendix A. Supplementary data

Supplementary data to this article can be found online at https://doi.org/10.1016/j.jpha.2024.02.004.

References

[1] E.J. Kuipers, W.M. Grady, D. Lieberman, et al., Colorectal cancer, Nat. Rev. Dis. Primers 1 (2015), 15065.
[2] Z.H. Siddik, Cisplatin: Mode of cytotoxic action and molecular basis of resistance, Oncogene 22 (2003) 7265–7279.
[3] L. Galluzzi, L. Senovilla, I. Vitale, et al., Molecular mechanisms of cisplatin resistance, Oncogene 31 (2012) 1869–1883.
[4] C. Passirani, A. Vessières, G. La Regina, et al., Modulating undruggable targets to overcome cancer therapy resistance, Drug Resist. Updat. 60 (2022), 100788.
[5] S.K. Rehman, J. Haynes, E. Collignon, et al., Colorectal cancer cells enter a diapause-like DTP state to survive chemotherapy, Cell 184 (2021) 226–242.e21.
[6] S.V. Sharma, D.Y. Lee, B. Li, et al., A chromatin-mediated reversible drug-tolerant state in cancer cell subpopulations, Cell 141 (2010) 69–80.
[7] B.B. Liau, C. Sievers, L.K. Donohue, et al., Adaptive chromatin remodeling drives glioblastoma stem cell plasticity and drug tolerance, Cell Stem Cell 20 (2017) 233–246.e7.
[8] I. Puig, S.P. Tenbaum, I. Chicote, et al., TET2 controls chemoresistant slow-cycling cancer cell survival and tumor recurrence, J. Clin. Invest. 128 (2018) 3887–3905.
[9] M. Malumbres, Cyclin-dependent kinases, Genome Biol. 15 (2014), 122.
[10] N. Rhind, P. Russell, Signaling pathways that regulate cell division, Cold Spring Harb. Perspect. Biol. 4 (2012), a005942.
[11] C. Trovesi, N. Manfrini, M. Falcettoni, et al., Regulation of the DNA damage response by cyclin-dependent kinases, J. Mol. Biol. 425 (2013) 4756–4766.
[12] J.M. Suski, N. Ratnayeke, M. Braun, et al., CDC7-independent G1/S transition revealed by targeted protein degradation, Nature 605 (2022) 357–365.
[13] L. Sisinni, F. Maddalena, V. Condelli, et al., TRAP1 controls cell cycle G2-M transition through the regulation of CDK1 and MAD2 expression/ubiquitination, J. Pathol. 243 (2017) 123–134.
[14] A. Recasens, L. Munoz, Targeting cancer cell dormancy, Trends Pharmacol. Sci. 40 (2019) 128–141.
[15] S.H. Chen, W.T. Huang, W. Kao, et al., O^6-methylguanine-DNA methyltransferase modulates cisplatin-induced DNA double-strand breaks by targeting the homologous recombination pathway in nasopharyngeal carcinoma, J. Biomed. Sci. 28 (2021), 2.
[16] R.R. White, J. Vijg, Do DNA double-strand breaks drive aging? Mol. Cell 63 (2016) 729–738.
[17] R. Scully, A. Panday, R. Elango, et al., DNA double-strand break repair-pathway choice in somatic mammalian cells, Nat. Rev. Mol. Cell Biol. 20 (2019) 698–714.
[18] E. Convery, E.K. Shin, Q. Ding, et al., Inhibition of homologous recombination by variants of the catalytic subunit of the DNA-dependent protein kinase (DNA-PKcs), Proc. Natl. Acad. Sci. U S A 102 (2005) 1345–1350.
[19] D. Ghosh, S.C. Raghavan, Nonhomologous end joining: New accessory factors fine tune the machinery, Trends Genet. 37 (2021) 582–599.
[20] L.S. Symington, J. Gautier, Double-strand break end resection and repair pathway choice, Annu. Rev. Genet. 45 (2011) 247–271.
[21] W. Yu, L. Zhang, Q. Wei, et al., O^6-methylguanine-DNA methyltransferase (MGMT): Challenges and new opportunities in glioma chemotherapy, Front. Oncol. 9 (2020), 1547.
[22] S.A. Abdellatief, A.A. Galal, S.M. Farouk, et al., Ameliorative effect of parsley oil on cisplatin-induced hepato-cardiotoxicity: A biochemical, histopathological, and immunohistochemical study, Biomed. Pharmacother. 86 (2017) 482–491.
[23] B.S. Moon, M. Cai, G. Lee, et al., Epigenetic modulator inhibition overcomes temozolomide chemoresistance and antagonizes tumor recurrence of glioblastoma, J. Clin. Invest. 130 (2020) 5782–5799.
[24] D.S. Malley, R.A. Hamoudi, S. Kocialkowski, et al., A distinct region of the MGMT CpG island critical for transcriptional regulation is preferentially methylated in glioblastoma cells and xenografts, Acta Neuropathol 121 (2011) 651–661.
[25] M. Wickström, C. Dyberg, J. Milosevic, et al., Wnt/β-catenin pathway regulates *MGMT* gene expression in cancer and inhibition of Wnt signalling prevents chemoresistance, Nat. Commun. 6 (2015), 8904.
[26] J. Raisch, A. Côté-Biron, M.J. Langlois, et al., Unveiling the roles of low-density lipoprotein receptor-related protein 6 in intestinal homeostasis, regeneration and oncogenesis, Cells 10 (2021), 1792.
[27] G. Emons, M. Spitzner, S. Reineke, et al., Chemoradiotherapy resistance in colorectal cancer cells is mediated by Wnt/β-catenin signaling, Mol. Cancer Res. 15 (2017) 1481–1490.
[28] J. Wang, H. Min, B. Hu, et al., Guanylate-binding protein-2 inhibits colorectal cancer cell growth and increases the sensitivity to paclitaxel of paclitaxel-resistant colorectal cancer cells by interfering Wnt signaling, J. Cell. Biochem. 121 (2020) 1250–1259.
[29] N. Kugimiya, A. Nishimoto, T. Hosoyama, et al., The c-MYC-ABCB5 axis plays a pivotal role in 5-fluorouracil resistance in human colon cancer cells, J. Cell. Mol. Med. 19 (2015) 1569–1581.
[30] R. Patro, G. Duggal, M.I. Love, et al., Salmon provides fast and bias-aware quantification of transcript expression, Nat. Methods 14 (2017) 417–419.
[31] Y. Zhou, B. Zhou, L. Pache, et al., Metascape provides a biologist-oriented resource for the analysis of systems-level datasets, Nat. Commun. 10 (2019), 1523.
[32] M.I. Love, W. Huber, S. Anders, Moderated estimation of fold change and dispersion for RNA-seq data with DESeq2, Genome Biol. 15 (2014), 550.
[33] B. Kaina, M. Christmann, S. Naumann, et al., MGMT: Key node in the battle against genotoxicity, carcinogenicity and apoptosis induced by alkylating agents, DNA Repair 6 (2007) 1079–1099.
[34] T. Iyama, D.M. Wilson 3rd, DNA repair mechanisms in dividing and non-dividing cells, DNA Repair 12 (2013) 620–636.
[35] A.E. Pegg, Multifaceted roles of alkyltransferase and related proteins in DNA repair, DNA damage, resistance to chemotherapy, and research tools, Chem. Res. Toxicol. 24 (2011) 618–639.
[36] K.A. van Nifterik, J. van den Berg, W.F. van der Meide, et al., Absence of the MGMT protein as well as methylation of the MGMT promoter predict the sensitivity for temozolomide, Br. J. Cancer 103 (2010) 29–35.
[37] R. Sancho, A.S. Nateri, A.G. de Vinuesa, et al., JNK signalling modulates intestinal homeostasis and tumourigenesis in mice, EMBO J. 28 (2009) 1843–1854.
[38] K.H. Goss, J. Groden, Biology of the adenomatous polyposis coli tumor suppressor, J. Clin. Oncol. 18 (2000) 1967–1979.
[39] S. Munemitsu, I. Albert, B. Souza, et al., Regulation of intracellular beta-catenin levels by the adenomatous polyposis coli (APC) tumor-suppressor protein, Proc. Natl. Acad. Sci. U S A 92 (1995) 3046–3050.